Influence of Strain Rate Sensitivity on Localization and Void Coalescence

Javier Reboul[a], Ankit Srivastava[b], Shmuel Osovski[c], Guadalupe Vadillo[a,*]

[a] *Department of Continuum Mechanics and Structural Analysis, University Carlos III of Madrid, Avda. de la Universidad, 30, 28911 Leganés, Madrid, Spain*
[b] *Department of Materials Science and Engineering, Texas A&M University, College Station, TX, USA*
[c] *Faculty of Mechanical Engineering, Technion-Israel Institute of Technology, Haifa, Israel*

Abstract

The onset of macroscopic strain localization limits the ductility of many ductile materials. For porous ductile materials, two distinct mechanisms of macroscopic localization have been identified: void growth induced softening and void coalescence. In this work we focus on analyzing the influence of materials strain rate sensitivity (SRS) on the two mechanisms of macroscopic localization or ductile failure as a function of the imposed stress triaxiality. To this end, three dimensional finite element calculations of unit cells have been carried out to model void growth and coalescence in an infinite block containing a periodic distribution of initially spherical voids in a band. The matrix material of the unit cell is considered to follow a strain rate dependent elastic perfectly plastic flow response. The unit cell calculations are carried out for a range of SRS parameter, imposed stress triaxiality and initial orientations of the voided band. Our results show that both the critical porosity and strain at the onset of localization and coalescence are strongly influenced by the SRS parameter and the imposed stress triaxiality values. Furthermore, the relative effect of the SRS parameter is found to increases with the increasing value of the imposed stress triaxiality.

Keywords: Ductility (A), Fracture Mechanisms (A), Elastic-viscoplastic Material (B), Porous Material (B), Finite Elements (C)

1. Introduction

The ductility of metals and alloys is limited by the onset of macroscopic strain localization, as it marks the end of uniform deformation and acts as a precursor to failure. Two distinct mechanisms have been identified that can lead to macroscopic strain localization in porous ductile materials (Tekoğlu et al., 2015).

The first mechanism of macroscopic strain localization involves strain softening due to microstructural changes, thermal effects and/or damage evolution resulting in local degradation in material's load carrying capacity. The local degradation in the material's load carrying capacity, causes localized deformation in a thin band with smoothly varying deformation pattern outside the

* *Email address:* gvadillo@ing.uc3m.es (Guadalupe Vadillo)

band (Fressengeas and Molinari, 1985; Tvergaard, 1981; Pardoen and Hutchinson, 2000; Mercier and Molinari, 2003; Aretz, 2007; Pineau et al., 2016). This results in a weak discontinuity along the thin band at the micro-scale and a discontinuity in the displacement field at the macro-scale. In porous ductile materials, damage (void growth) induced softening is the dominant mechanism that triggers the onset of macroscopic localization (Tvergaard, 1982), resulting in void sheet fracture. The width of the thin band engulfing the voids in this scenario has a length scale comparable or greater than the mean spacing between the voids. Under these circumstances the onset of macroscopic localization is strongly dependent on material properties, initial porosity, orientation of the band undergoing localized deformation and the imposed stress state (Needleman and Rice, 1978; Yamamoto, 1978).

The second mechanism of macroscopic strain localization in porous ductile materials involves void coalescence. Void coalescence is a local instability phenomenon where the interaction between neighboring voids plays a critical role. The onset of void coalescence is associated with a sudden concentration of plastic strain in the ligaments linking neighboring voids (Koplik and Needleman, 1988). Thus, following the onset of void coalescence, the kinematics of the void enlargement significantly differs from that of void growth prior to this instability mode. For void coalescence induced macroscopic localization the width of the micro-scale localization band is much more narrower because the deformation is limited to the ligaments between the neighbouring voids.

The two aforementioned mechanisms of macroscopic localization in porous ductile materials, void growth induced softening and void coalescence, are distinct and have been identified in Tekoğlu et al. (2015); Guo and Wong (2018). In particular, for a strain rate independent material, Tekoğlu et al. (2015) showed that depending on the value of the imposed stress triaxiality a clear separation exists between the two mechanisms of macroscopic localization. This raises a fundamental question: how does the material's strain rate sensitivity affect the two mechanisms of macroscopic localization or ductile failure as a function of the imposed stress triaxiality?

The strain rate sensitivity is an important material parameter and it greatly affects the onset of localized deformation and damage evolution (Marciniak et al., 1973; Hutchinson and Neale, 1977; Ghosh, 1977; Hutchinson et al., 1978; Taya and Seidel, 1981; Budiansky et al., 1982; Cocks and Ashby, 1982a,b; Pan, 1983a; Pan et al., 1983; Yoon and Taya, 1984; Duva, 1986; Nemat-Nasser et al., 1986; Ortiz and Molinari, 1992; Czarnota et al., 2006; Vadillo et al., 2012; Srivastava and Needleman, 2013; Agoras and Ponte Castañeda, 2014; Osovski et al., 2015; Wang et al., 2018). This in turn affects the performance, safety, reliability and manufacturability of engineering components and structures; for example, the crash worthiness of automobiles, the blast resistance of ships and airplane cargo holds, and the manufacturability of sheet metal components. In general, increasing the strain rate sensitivity of a ductile material can delay the onset of localized plastic deformation. Furthermore, it has also been shown that an increase in the material's strain rate sensitivity can slow down the evolution of porosity and delay the onset of void coalescence in a porous ductile material. In this work we focus on analyzing the influence of materials strain rate sensitivity on the two mechanisms of macroscopic localization or ductile failure as a function of the imposed stress triaxiality.

Several analytical and computational studies have been carried out in past to analyze the onset of localized deformation (Marciniak and Kuczyński, 1967; Rudnicki and Rice, 1975; Rice, 1977; Saje et al., 1982; Pan, 1983b; Mear and Hutchinson, 1985; Nahshon and Hutchinson, 2008). The micro-mechanical approach that constitute the basis of these works involves analyzing an

infinite sheet or block with a defect band inclined at an angle with respect to the imposed loading direction. Alternatively, the onset of localization in a porous material can also be analyzed via unit cell model calculations. In the unit cell model calculations, a periodic distribution of voids in the material is assumed, that allows us to model a single void in the material and impose proportional loading throughout the deformation history (Koplik and Needleman, 1988; Scheyvaerts et al., 2011; Fritzen et al., 2012; Srivastava and Needleman, 2013; Brünig et al., 2013; Dunand and Mohr, 2014; Tekoğlu et al., 2015; Liu et al., 2016; Torki et al., 2017; Guo and Wong, 2018; Luo and Gao, 2018). Thus, unit cell model calculations not only provide the macroscopic response of the material but also provide the details of the void growth and coalescence, as a function of the imposed constant stress triaxiality values.

In this work, three dimensional finite element calculations of unit cells have been carried out to model macroscopic strain localization due to damage induced softening, void growth and/or coalescence, in an infinite block containing a periodic distribution of initially spherical voids in a band. Note that we have assumed a state of the material where either the voids are initially present or have already nucleated (uniformly for the sake of simplicity) in a narrow region in the material. The unit cell modeled consists of a central block with a single void in its center within two semi-infinite void-free blocks. The matrix material of the unit cell is considered to follow a strain rate dependent elastic perfectly plastic flow response. Limited calculations have also been carried out to explore the combined effect of material's strain rate sensitivity and strain hardening. The unit cell calculations are carried out for one initial void volume fraction, a range of strain rate sensitivity parameter, a range of imposed stress triaxiality, and three initial orientations of the voided band. In the calculations, onset of macroscopic localization is defined as the point when the ratio of the rate of deformation in the band and outside the band reaches a critical level, while the onset of void coalescence is defined when the ratio of the maximum to the minimum effective plastic strain rate at the surface of the void reaches a critical value following the work of Tekoğlu et al. (2015); Guo and Wong (2018).

The remainder of this paper are organized as follows. The problem formulation and numerical method are detailed in Section 2. The numerical results and the discussion of the key results are presented in Section 3. The main conclusions of this work are summarized in Section 4.

2. Problem Formulation and Numerical Method

Three dimensional finite element calculations are carried out to model plastic flow localization and void coalescence in an infinite block containing a periodic distribution of initially spherical voids in a band as shown in Fig. 1 (top left). The configuration analyzed here is numerically similar to the works of Tvergaard (1989); Barsoum and Faleskog (2011); Tekoğlu et al. (2015) and Guo and Wong (2018).

2.1. Unit Cell Model

As shown in Fig. 1, for the periodic distribution of the voids in the voided band, a unit cell can be defined as a central block with a single void in its center within two void-free semi-infinite blocks. The initial volume of the central block is taken to be $V_{central\ block} = D_{10}D_{20}D_{30} = D_0^3$ and the initial volume fraction of the spherical void with radius R_0 is $f_0 = 4\pi R_0^3/3D_0^3$. In the finite element calculations, the semi-infinite blocks along x_1 direction are assumed to be of finite

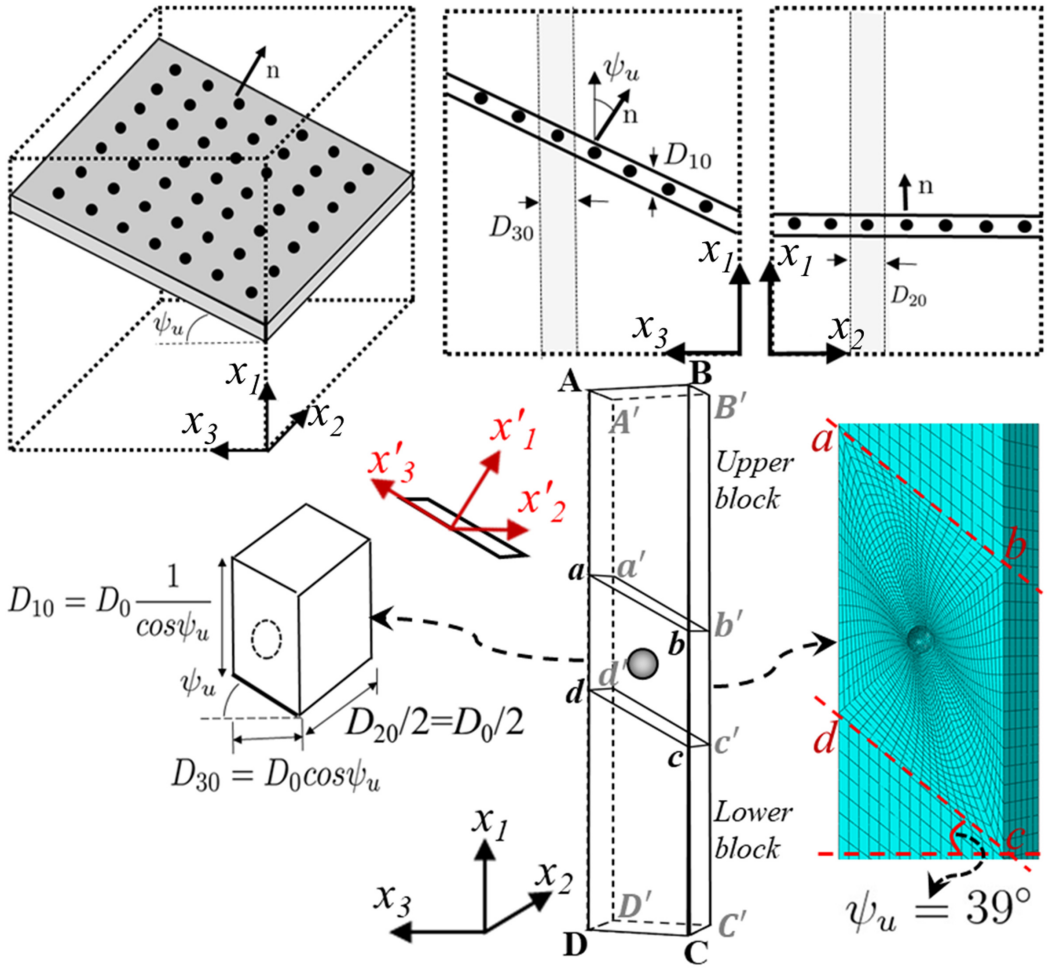

Figure 1: Three dimensional representation of an infinite block containing a periodic distribution of initially spherical voids in a band initially inclined at an angle ψ_u with respect to the x_2-x_3 plane (top left). The two dimensional sections of the block along x_1-x_3 (top center) and x_1-x_2 (top right) planes are also shown in the figure to highlight the periodicity of the voids. Owing to the periodic distribution of the voids, the voided band can be represented as a central block with a single void in its center within two void-free semi-infinite blocks (bottom center). The initial dimensions of the central block are D_{10}, D_{20}, and D_{30} along x_1, x_2 and x_3 axes, respectively (bottom left). A zoomed in view of the finite element model of 1/2 unit cell with initial void volume fraction, $f_0 = 0.001$ and $\psi_u = 39°$ (bottom right).

length but long enough to numerically mimic semi-infinite blocks. For a given loading state and orientation angle, ψ_u, of the voided band in the initial state, the orientation angle of the band at any deformation angle ψ progress with the deformation of the outer blocks as:

$$\tan(\psi) = e^{(E_1 - E_3)} \tan(\psi_u) \tag{1}$$

$$\dot{\psi} = \frac{1}{2} \sin(2\psi) \left(\dot{E}_1 - \dot{E}_3 \right) \tag{2}$$

where, E_1, E_2, E_3, are the macroscopic logarithmic principal strains given as:

$$E_1 = \ln(\lambda_1), \quad E_2 = \ln(\lambda_2), \quad E_3 = \ln(\lambda_3) \tag{3}$$

In Eq. (3), $\lambda_1 = L_1/L_{10}$, $\lambda_2 = L_2/L_{20}$ and $\lambda_3 = L_3/L_{30}$, with L_{i0} being the initial, and L_i being the current lengths of the unit cell along x_i axes. The current lengths of the unit cell follow,

$$L_1 = L_{10} + U_1; \quad L_2/2 = L_{20}/2 + U_2; \quad L_3 = L_{30} + U_3 \tag{4}$$

where, U_i, are taken at point A' in Fig. 1. Following Eq. (3), the rates of macroscopic logarithmic principal strains are:

$$\dot{E}_1 = \frac{\dot{\lambda}_1}{\lambda_1}, \quad \dot{E}_2 = \frac{\dot{\lambda}_2}{\lambda_2}, \quad \dot{E}_3 = \frac{\dot{\lambda}_3}{\lambda_3} \tag{5}$$

The unit cell shown in Fig. 1 (bottom) is symmetric along x_2 axis, so that only 1/2 of the unit cell needs to be analyzed. The boundary conditions $u_2^{ABba} = u_2^{abcd} = u_2^{dcCD} = 0$ and $u_2^{A'B'b'a'} = u_2^{a'b'c'd'} = u_2^{d'c'C'D'} = U_2$ are imposed on the external faces of the unit cell normal to x_2 axis. Also, we assume that the external faces of the upper and lower blocks of the unit cell (see Fig. 1) that are initially straight and normal to the x_1 and x_3 axes remain normal and straight throughout the deformation history. This results in boundary conditions, $u_1^{DD'C'C} = 0$ and $u_1^{AA'B'B} = U_1$, and $u_3^{BB'b'b} = u_3^{cc'C'C} = 0$ and $u_3^{AA'a'a} = u_3^{dd'D'D} = U_3$. Next, following Tvergaard (1989), boundary conditions applied on the external faces of the band in the unit cell that are initially straight and normal to the x_3 axis are,

$$\begin{aligned} u_1^{aa'd'd} - u_1^{bb'c'c} &= L_{30}\left(e^{E_3}\tan(\psi) - \tan(\psi_u)\right) \\ u_3^{aa'd'd} - u_3^{bb'c'c} &= L_{30}\left(e^{E_3} - 1\right) \end{aligned} \tag{6}$$

where, $L_{30} = D_{30} = D_0\cos(\psi_u)$.

The voided part of the cell is weaker than the outer blocks. This is reflected by additional rigid body displacements among the outer blocks with values $2\Delta_1$ and $2\Delta_3$. The values Δ_1 and Δ_3 vanish if the cell has no void. By symmetry, there is no relative displacement of the outer blocks in x_2 direction. The corresponding relative displacement field in the upper block outside the voided cell (evaluated at point a in Fig. 1 and relative to the center of the void) can then be given as:

$$\begin{aligned} u_1 &= (\lambda_1 - 1)\, x_1 + \Delta_1 \\ u_2 &= (\lambda_2 - 1)\, x_2 \\ u_3 &= (\lambda_3 - 1)\, x_3 + \Delta_3 \end{aligned} \tag{7}$$

The strain rate components in the band, $\dot{E}_{ij}^b$, are the result of the sum of the uniform strain outside the band plus the strain associated with the rigid body displacements Δ_1 and Δ_3:

$$\dot{E}_{11}^b = \cos^2(\psi)\,\dot{E}_1 + \sin^2(\psi)\,\dot{E}_3 + \frac{2\dot{\Delta}_1\cos(\psi) - 2\dot{\Delta}_3\sin(\psi)}{H}$$

$$\begin{aligned}
\dot{E}^b_{22} &= \dot{E}_2 \\
\dot{E}^b_{33} &= \sin^2(\psi)\,\dot{E}_1 + \cos^2(\psi)\,\dot{E}_3 \\
\dot{E}^b_{13} &= \sin(2\psi)\left(\dot{E}_1 - \dot{E}_3\right) + \frac{2\dot{\Delta}_3\cos(\psi) + 2\dot{\Delta}_1\sin(\psi)}{H}
\end{aligned} \tag{8}$$

Here, the components of $\dot{E}^b_{ij}$ are defined with respect to the local axes (x'_1, x'_2, x'_3) attached to the band that consequently rotates with the band.

The components of the strain rate $\dot{E}_{ij}$ are however expressed with respect to x_1, x_2 and x_3 axes. H is the current thickness of the band (in x'_1 direction), being $H_0 = D_{10}cos\psi_u$, with $\dot{H} = \dot{E}^b_{11}H$.

The $\dot{E}^b_{eq}$ and $\dot{E}_{eq}$ are given as:

$$\dot{E}^b_{eq} = \sqrt{\frac{2}{3}\dot{E}^b_{ij}\dot{E}^b_{ij}}, \quad \dot{E}_{eq} = \sqrt{\frac{2}{3}\left(\dot{E}_1^2 + \dot{E}_2^2 + \dot{E}_3^2\right)} \tag{9}$$

and, $E^b_{eq} = \int_0^t \dot{E}^b_{eq}d\tau$ and $E_{eq} = \int_0^t \dot{E}_{eq}d\tau$.

The macroscopic true principal stresses Σ_1, Σ_2 and Σ_3, or the average reaction forces per unit area at the deformed cell boundary, are defined in terms of the Cauchy stress components, σ_{ii}, as:

$$\Sigma_i = \frac{1}{L_jL_k}\int_0^{L_j}\int_0^{L_k}\left[\sigma_{ii}\right]_{x_i=L_i}dx_jdx_k \quad \text{with } i,j,k = 1,2,3$$

The macroscopic stress triaxiality, T, and the Lode parameter, L are defined as:

$$T = \frac{\Sigma_h}{\Sigma_{eq}}; \;\; L = \frac{2\Sigma_2 - \Sigma_1 - \Sigma_3}{\Sigma_1 - \Sigma_3} \tag{10}$$

with Σ_h and Σ_e being the hydrostatic and equivalent macroscopic stresses, respectively, and are given as:

$$\Sigma_h = \frac{\Sigma_1 + \Sigma_2 + \Sigma_3}{3}, \quad \Sigma_{eq} = \frac{1}{\sqrt{2}}\left(\left(\Sigma_1 - \Sigma_2\right)^2 + \left(\Sigma_1 - \Sigma_3\right)^2 + \left(\Sigma_2 - \Sigma_3\right)^2\right)^{1/2} \tag{11}$$

Relations, Eq. (10) and Eq. (11) allows to express Σ_1, Σ_2, Σ_3 as functions of Σ_{eq}, T and L, with the range of possible values:

$$0 \le \Sigma_e \le \infty, \;\; -\infty \le T \le \infty, \quad -1 \le L \le 1 \tag{12}$$

In this work, the stress states are characterized by the values of the stress triaxiality, T, and the Lode parameter L, while the strain states are characterized by the equivalent strain in the band, E^b_{eq}, and the macroscopic equivalent strain, E_{eq}, in the upper/lower faces of the outer blocks. Finite element unit cell calculations are carried out for prescribed constant stress triaxiality, T, and Lode parameter, L, values using the commercial finite element code ABAQUS/Standard (2017). The periodic boundary conditions on the faces of the unit cell are implemented as multi-point

constraints in ABAQUS/Standard (2017), while the boundary conditions required to prescribe constant values of T and L are implemented in ABAQUS/Standard (2017) using an MPC user defined subroutine. More details of the boundary conditions to prescribe constant values of T and L are given in Appendix A. The finite element calculations use C3D20R elements from the in-built element library of ABAQUS/Standard (2017), and the number of elements in the finite element mesh varies from $9,672$ to $18,316$ for initial band angle varying from $\psi_u = 0^\circ$ to 39°, respectively. A cropped region of a unit cell with $\psi_u = 39^\circ$, $f_0 = 0.001$ and $D_0 = 1\ mm$ with finite element mesh in the voided region is shown in Fig. 1.

2.2. Constitutive Relation

The matrix material of the unit cell is modeled using finite strain J_2 flow theory. In the finite element calculations, updated Lagrangian formulation is used to account for large deformations. For hypo elastic-plastic materials, the macroscopic rate of plastic deformation tensor, $\dot{\mathbf{E}}^p$, is assumed to be related to the macroscopic stress rate by:

$$\dot{\mathbf{\Sigma}} = \mathbf{C} : \left(\dot{\mathbf{E}} - \dot{\mathbf{E}}^p\right) \tag{13}$$

where, $\mathbf{C}$ is the linear isotropic elastic tensor defined by the fourth order tensorial relation:

$$\mathbf{C} = 2G\mathbf{I}_{dev} + K\mathbf{1} \otimes \mathbf{1} \tag{14}$$

with I_{dev} being the unit deviatoric fourth order tensor having the form,

$$(I_{dev})_{ijkl} = 1/2\left(\delta_{ik}\delta_{jl} + \delta_{il}\delta_{jk}\right) - 1/3\delta_{ij}\delta_{kl} \tag{15}$$

while $G = E/(2(1+\nu))$ and $K = E/(3(1-2\nu))$ are elastic constants.
Assuming Mises plasticity, the yield function and the associated flow rule are given as:

$$\begin{aligned} \Psi &= \Sigma_{eq} - \bar{\sigma}\left(\dot{\varepsilon}^p\right) \\ \dot{\mathbf{E}}^p &= \dot{\lambda}\frac{\partial \Psi}{\partial \dot{\mathbf{\Sigma}}} \end{aligned} \tag{16}$$

where, $\bar{\sigma}$ follows:

$$\bar{\sigma} = \begin{cases} E\varepsilon & \varepsilon \leq \varepsilon_0 \\ \sigma_0 \cdot (1 + (\frac{\dot{\varepsilon}^p}{\dot{\varepsilon}_0})^m) & \varepsilon > \varepsilon_0 \end{cases} \tag{17}$$

In Eq. (17), σ_0 represents a reference yield stress, m is the strain rate sensitivity parameter of the material, $\dot{\varepsilon}_0$ is the reference strain rate, E is the Young's modulus, $\varepsilon_0 = \sigma_0/E$, and plastic equivalent strain rate, $\dot{\varepsilon}^p = \sqrt{\frac{2}{3}\dot{\mathbf{E}}^p : \dot{\mathbf{E}}^p}$.

3. Results and Discussion

In a porous ductile material, onset of macroscopic localization due to the softening induced by void nucleation and growth, or due to void coalescence resulting from plastic strain localization in the ligaments between the voids, marks the end of uniform deformation. For a strain rate independent porous ductile material, Tekoğlu et al. (2015) showed that depending on the value of the imposed stress triaxiality a clear separation exists between the two modes of macroscopic localization. This raises a fundamental question: how does the material's strain rate sensitivity affect the two modes of localization or ductile failure as a function of the imposed stress triaxiality? In this section, we present results obtained using the numerical method detailed under Section 2 to address this question.

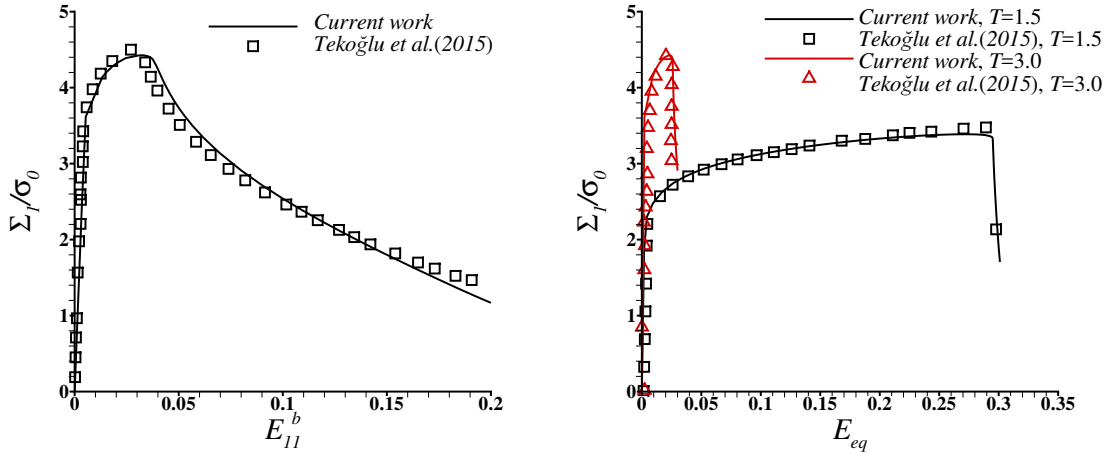

(a) (b)

Figure 2: Comparison of the evolution of (a) normalized Σ_1/σ_0 with E^b_{11} for $T = 3.0$ and that of (b) Σ_1/σ_0 with E_{eq} for $T = 1.5$ and $T = 3.0$, predicted in the current work with the results of Tekoğlu et al. (2015). In both (a) and (b), $L = -1$, $\psi_u = 0°$, $f_0 = 0.001$ and $N = 0.1$.

Our numerical method to model the unit cell that includes a central block with a single void in its center within two void-free semi-infinite blocks, differs from that of Tekoğlu et al. (2015). Tekoğlu et al. (2015) only considered the inclined part of the unit cell within the band, Fig. 1, and modeled the void-free semi-infinite block (along x_1) through complex boundary conditions. On the other hand, here we assume that (see Section 2) if the length of the void-free block along x_1 is sufficiently greater than the characteristic length, D_0, of the unit cell, it can mimic the semi-infinite block. Thus, it is warranted to validate the predictions of our numerical method against the available results of Tekoğlu et al. (2015). To this end, we use a strain rate independent flow response, as in Tekoğlu et al. (2015):

$$\bar{\sigma} = \begin{cases} E\varepsilon & \varepsilon \leq \varepsilon_0 \\ \sigma_0 \cdot (\frac{\varepsilon^p}{\varepsilon_0})^N & \varepsilon > \varepsilon_0 \end{cases} \tag{18}$$

instead of Eq. (17). The calculations use, $E = 167GPa$, $\sigma_0 = 418MPa$, $\varepsilon_0 = 0.0025$, $\nu = 0.3$ and $N = 0.1$. The evolution of the normalized macroscopic stress along x_1, Σ_1/σ_0, with the strain

in the band, E^b_{11}, for $T = 3.0$, $L = -1$, $\psi_u = 0^\circ$ and $f_0 = 0.001$ predicted using the numerical method detailed under Section 2 are compared with the results of Tekoğlu et al. (2015) in Fig. 2(a). Similarly, the evolution of Σ_1/σ_0 with the macroscopic equivalent strain in the outer blocks, E_{eq}, for $T = 1.5$ and 3.0, and the same values of L, ψ_u and f_0 predicted using the current method are compared with the results of Tekoğlu et al. (2015) in Fig. 2(b). The results (of the current work) presented in Fig. 2, are for a unit cell whose length along x_1 direction is six times the characteristic length, D_0, of the problem i.e. $L_{10} = 6D_0$. The strikingly good correlation between the predictions using our method and the results of Tekoğlu et al. (2015) in Fig. 2, clearly shows that the assumption of $L_{10} = 6D_0$ numerically represent the unit cell consisting of a central block with a single void in its center within two void-free semi-infinite blocks.

After validating our numerical method, we now focus on analyzing the influence of material's strain rate sensitivity on the onset of macroscopic localization due to void growth induced softening and/or void coalescence. All the results presented here onwards are from the finite element calculations utilizing strain rate dependent flow response defined in Eq. (17). The full set of constitutive parameters used to define material (in the band as well as in the outer block) in the calculations are: $E = 167GPa$, $\nu = 0.3$, $\sigma_0 = 418MPa$, $\varepsilon_0 = 0.0025$, and $\dot{\varepsilon}_0 = 1\ s^{-1}$, while the strain rate sensitivity parameter, m, is varied from 0 to 0.25. For each strain rate sensitivity parameter value, unit cells with one initial void volume fraction, $f_0 = 0.001$, but three initial orientations of the voided band, $\psi_u = 0^\circ$, 20° and 39° are considered. The choice of the initial orientation of the voided band, ψ_u, is based on the results of Tekoğlu et al. (2015) for strain rate independent material. Finally, for each strain rate sensitivity parameter, m, value and initial orientation of the voided band, ψ_u, calculations are carried out for prescribed constant stress triaxiality, T, values in the range, $0.75 \leq T \leq 3$ and one Lode parameter, $L = -1$.

3.1. Strain Localization, Void Growth and Void Coalescence

The evolution of the equivalent strain inside the band, E^b_{eq}, with the macroscopic equivalent strain outside the band, E_{eq}, in unit cells with initial orientation of the voided band, $\psi_u = 0^\circ$ and 39° are shown in Fig. 3. As shown in Figs. 3, during initial stages of deformation E^b_{eq} is same as E_{eq}, but at later stages of deformation, strain localizes in the band, and thereafter E^b_{eq} increases rapidly while E_{eq} increases slightly in the material outside the band. The onset of localization is assumed to occur when the ratio between the rate of macroscopic equivalent strain in the band and outside the band reach the value of 5. The onset of void coalescence is assumed to occur when the ratio of the maximum to the minimum equivalent plastic strain rate at the void surface first exceeds the threshold of 20, as in Tekoğlu et al. (2015). For $T = 1.25$, the onset of coalescence occurs soon after the onset of localization. But, for $T = 2.75$, the onset of coalescence occurs at a much greater value of E^b_{eq} following the onset of localization. A comparison of the results shown in Figs. 3(a) and (b), and Figs. 3(c) and (d), show that increasing the strain rate sensitivity of the material delays the onset of both, the localization and coalescence. However, the relative stabilizing effect of material's strain rate sensitivity is greater at the onset of localization than at the onset of void coalescence. For example, for $T = 2.75$, $(E^b_{eq})_{m=0.25}/(E^b_{eq})_{m=0} \approx 5.3$ at the onset of localization and $(E^b_{eq})_{m=0.25}/(E^b_{eq})_{m=0} \approx 2.8$ at the onset of void coalescence. Also a comparison of the results shown in Figs. 3(a) and (c), and Figs. 3(b) and (d), show that there is an increase in the relative stabilizing effect of material's strain rate sensitivity with the increasing value of the imposed stress triaxiality.

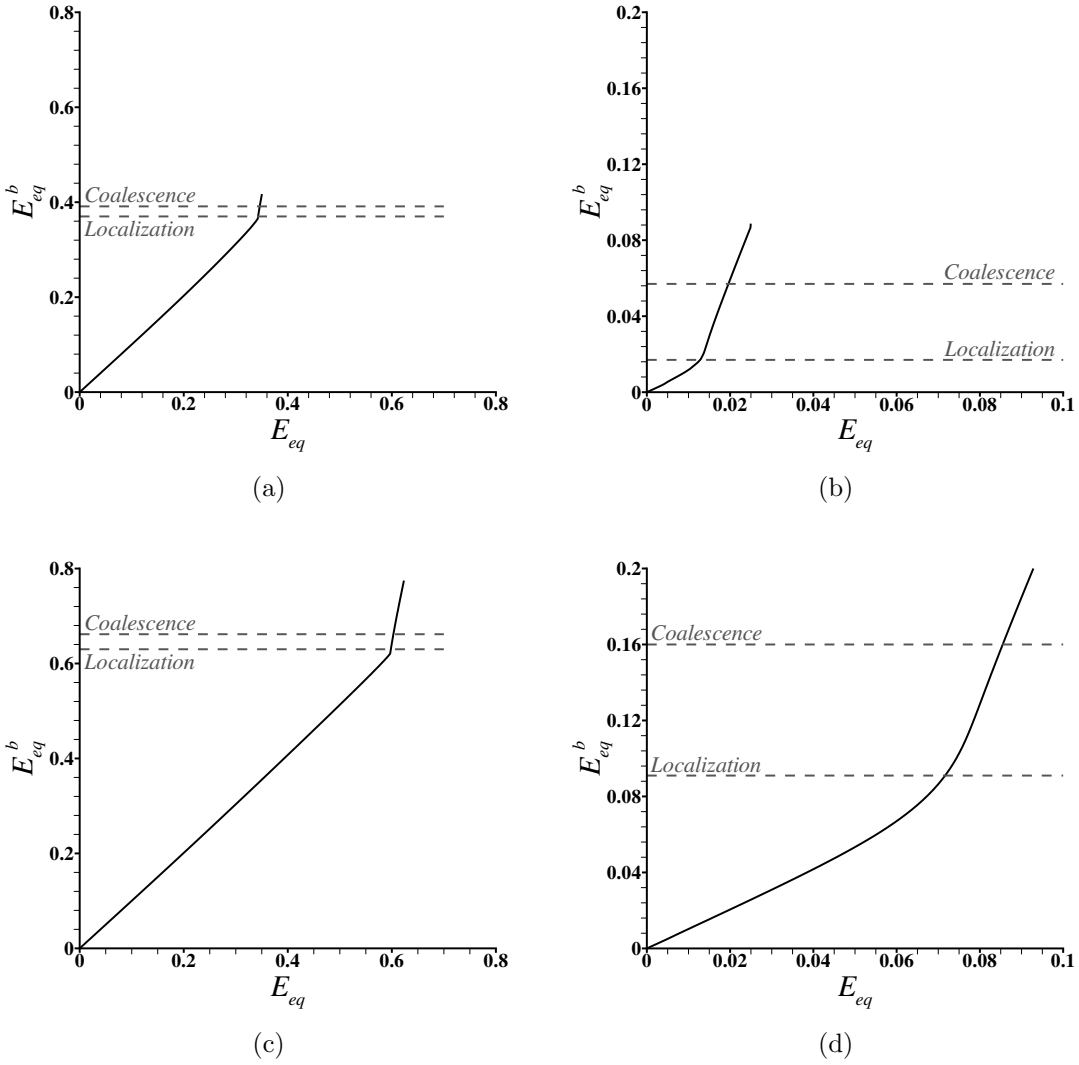

Figure 3: Evolution of equivalent strain in the band, E^b_{eq}, with macroscopic equivalent strain outside the band, E_{eq}, for (a) imposed stress triaxiality, $T = 1.25$ and strain rate sensitivity parameter, $m = 0$, (b) $T = 2.75$ and $m = 0$, (c) $T = 1.25$ and $m = 0.25$, and (d) $T = 2.75$ and $m = 0.25$. The initial orientation of the voided band is $\psi_u = 0^\circ$ for the cases shown in (a) and (c), and $\psi_u = 39^\circ$ for the cases shown in (b) and (d). In the figures the value of E^b_{eq} at the onset of localization and void coalescence are marked with dashed horizontal lines.

The evolution of normalized porosity, f/f_0, with macroscopic equivalent strain outside the band, E_{eq}, for $T = 1.25$, is shown for two unit cells with initial orientation of the voided band $\psi_u = 0^\circ$ and $\psi_u = 39^\circ$ in Figs. 4(a) and (c), respectively. The same is shown for $T = 2.5$, for two unit cells with $\psi_u = 0^\circ$ and $\psi_u = 39^\circ$ in Figs. 4(b) and (d), respectively. To quantify the influence of the strain rate sensitivity parameter on the evolution of the porosity, results are shown in Fig. 4 for $m = 0,\ 0.05$, and 0.1. As shown in Fig. 4, for both the values of T and ψ_u, a higher value of m shifts the f/f_0 versus E_{eq} curves to the right i.e. the stabilizing effect of the material's strain rate sensitivity slows down the evolution of porosity. For $T = 2.5$, the value of f/f_0 at the onset of localization is less than the value of f/f_0 at the onset of void coalescence for both the values

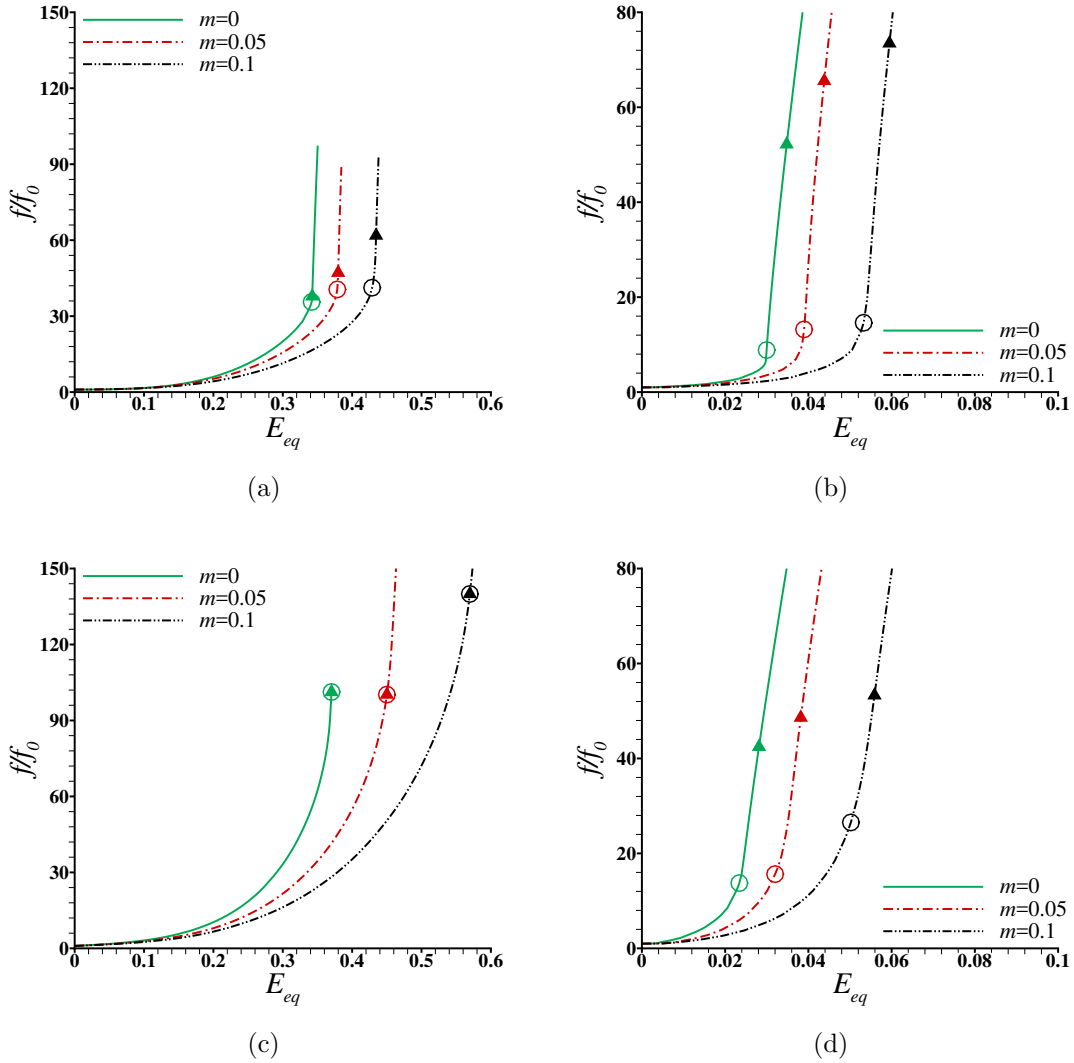

Figure 4: Evolution of the normalized porosity, f/f_0, with E_{eq} for (a) $\psi_u = 0°$ and $T = 1.25$, (b) $\psi_u = 0°$ and $T = 2.5$, (c) $\psi_u = 39°$ and $T = 1.25$, and (d) $\psi_u = 39°$ and $T = 2.5$. The open circles in the figure mark the onset of localization while the closed triangles mark the onset of void coalescence.

of ψ_u and all three values of m. For $T = 1.25$, the value of f/f_0 at the onset of localization is less than the value of f/f_0 at the onset of void coalescence for $\psi_u = 0°$ for $m > 0$. However, for $T = 1.25$, the value of f/f_0 at the onset of localization is same as the value of f/f_0 at the onset of void coalescence for $\psi_u = 39°$ for all three values of m.

The effect of the material's strain rate sensitivity on deformation in the band and distribution of equivalent plastic strain on the void surface is highlighted in Fig. 5. In Fig. 5, results are shown for two strain rate sensitivity parameters, $m = 0$ and 0.25, for a unit cell with the initial orientation of the band, $\psi_u = 20°$ and subjected to an imposed stress triaxiality, $T = 1.0$. As can be seen in Fig. 5, the edges, ad and bc, that were initially straight and normal to the x_3 axis, undergo deformation following the periodicity of the initial voids in the band. In addition, the results also show that at the same equivalent strain levels in the band, E^b_{eq}, the maximum value

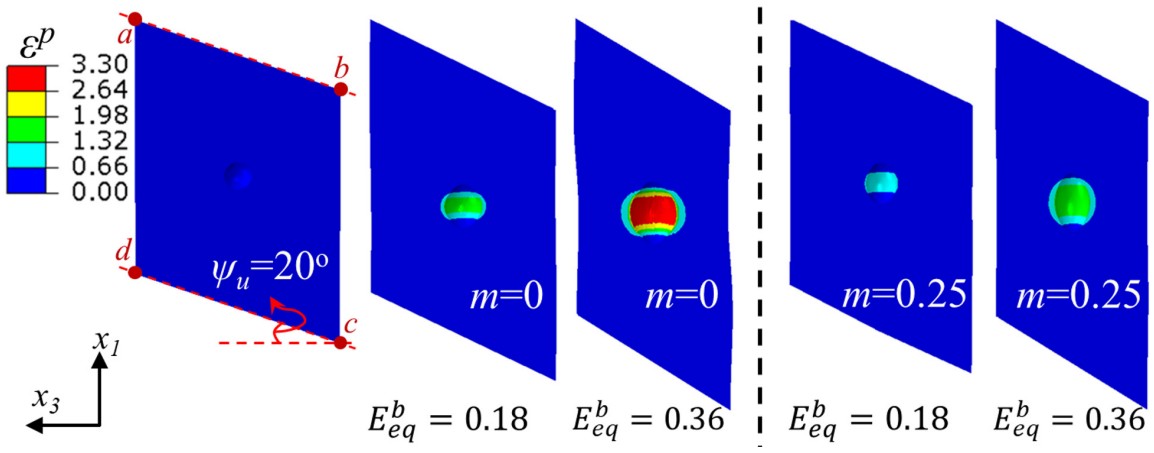

Figure 5: Deformed shape of the band and the distribution of the equivalent plastic strain, ε^p, in the band with initial orientation $\psi_u = 20°$ under imposed stress triaxiality $T = 1.0$ for two strain rate sensitivity parameters, $m = 0$ and 0.25 at two equivalent strain levels in the band, $E^b_{eq} = 0.18$ and 0.36.

of equivalent plastic strain, ε^p, on the void surface for $m = 0.25$ is much less than that for $m = 0$. The lower levels of ε^p on the void surface for $m = 0.25$ compared to $m = 0$ is consistent with the effect of m on the evolution of f/f_0 shown in Fig. 4.

3.2. Effect of Strain Rate Sensitivity on Critical Porosity

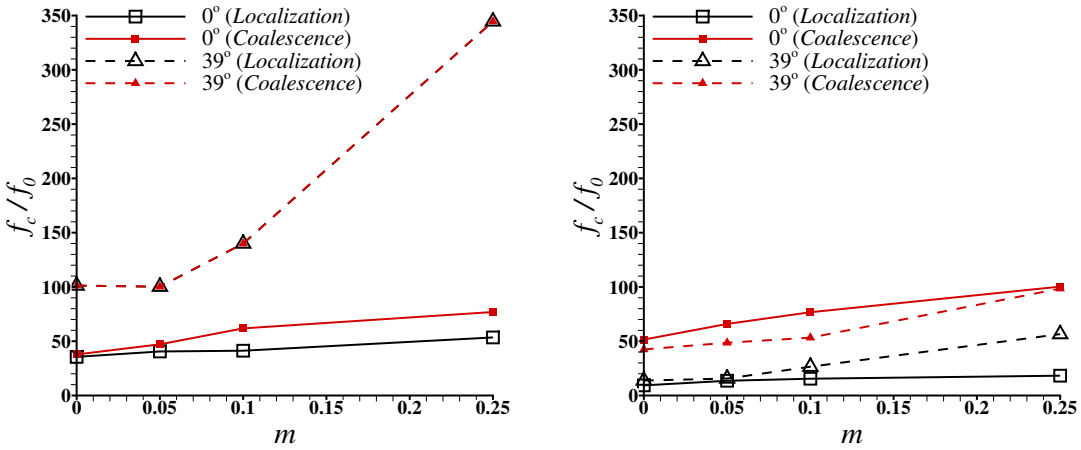

Figure 6: Variation of the normalized critical value of porosity, f_c/f_0, at the onset of localization and void coalescence with material's strain rate sensitivity parameter, m, for (a) $T = 1.25$ and (b) $T = 2.5$.

We now analyze the effect of material's strain rate sensitivity, m, on critical values of porosity at the onset of strain localization and void coalescence. The critical value of porosity at the onset of void coalescence is widely used as an input parameter to simulate ductile fracture due to void nucleation, growth and coalescence (Besson et al., 2003; Srivastava et al., 2014; Cheng et al., 2014).

The variation of the normalized critical value of porosity, f_c/f_0, at the onset of localization and void coalescence with material's strain rate sensitivity parameter, m, in two unit cells with initial orientation of the voided band, $\psi_u = 0°$ and 39°, for two values of imposed stress triaxiality, $T = 1.25$ and 2.5, are shown in Fig. 6. For $T = 1.25$ and $\psi_u = 0°$, the values of f_c/f_0 at the onset of localization and void coalescence are roughly the same for $m < 0.05$. However, for greater value of m the value of f_c/f_0 at the onset of localization is less than the value of f_c/f_0 at the onset of void coalescence. For $T = 1.25$ and $\psi_u = 39°$, the values of f_c/f_0 at the onset of localization and void coalescence are roughly the same for all values of m. On the other hand, for $T = 2.5$, the values of f_c/f_0 at the onset of localization is less than the values of f_c/f_0 at the onset of void coalescence for all values of m, for both $\psi_u = 0°$ and 39°. Also, for $T = 2.5$ the difference between the values of f_c/f_0 at the onset of localization and void coalescence increases with increasing value of m. The results presented in Fig. 6 show that at low imposed stress triaxiality values, the extent of void growth induced softening is not sufficient to trigger macroscopic localization, thus localization does not occur until the onset of void coalescence. On the other hand, the void growth induced softening is sufficient to trigger macroscopic localization at high imposed stress triaxiality values and the macroscopic localization occurs much before the void coalescence. The increase in the value of f_c with increasing value of m is because an increase in the value of m results in increased strain rate hardening thus requiring an increase in damage induced softening to trigger any localized deformation in the voided band or within the ligament between the neighboring voids to trigger void coalescence.

3.3. Effect of Strain Rate Sensitivity on Critical Strain

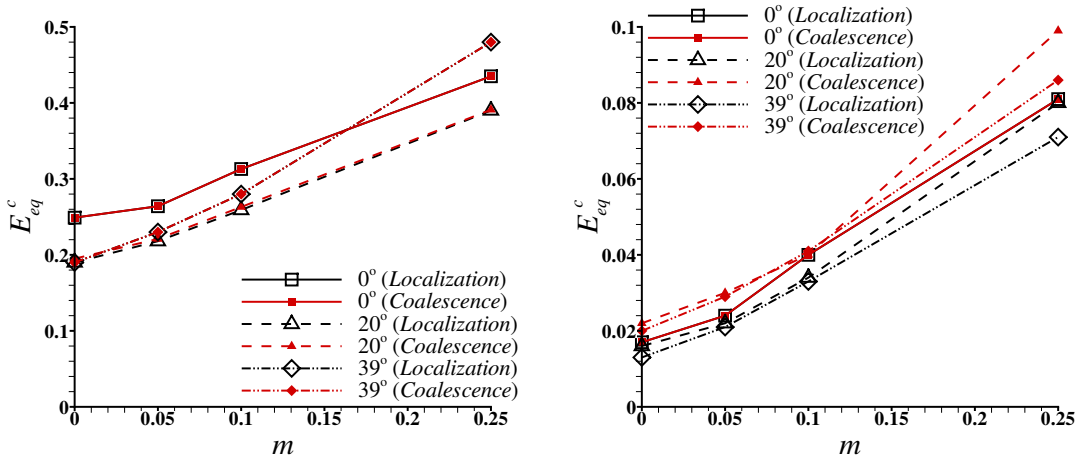

Figure 7: Variation of the critical macroscopic equivalent strain, E^c_{eq}, outside the band at the onset of localization/coalescence with material's strain rate sensitivity parameter, m, for (a) $T = 1.5$ and (b) $T = 2.75$.

The results presented thus far clearly show that both the material's strain rate sensitivity and imposed stress triaxiality affect the onset of strain localization and void coalescence. Following this, we analyze the variation of critical macroscopic equivalent strain outside the band, E^c_{eq}, and critical equivalent strain inside the band, E^{cb}_{eq}, with strain rate sensitivity parameter, m, shown in

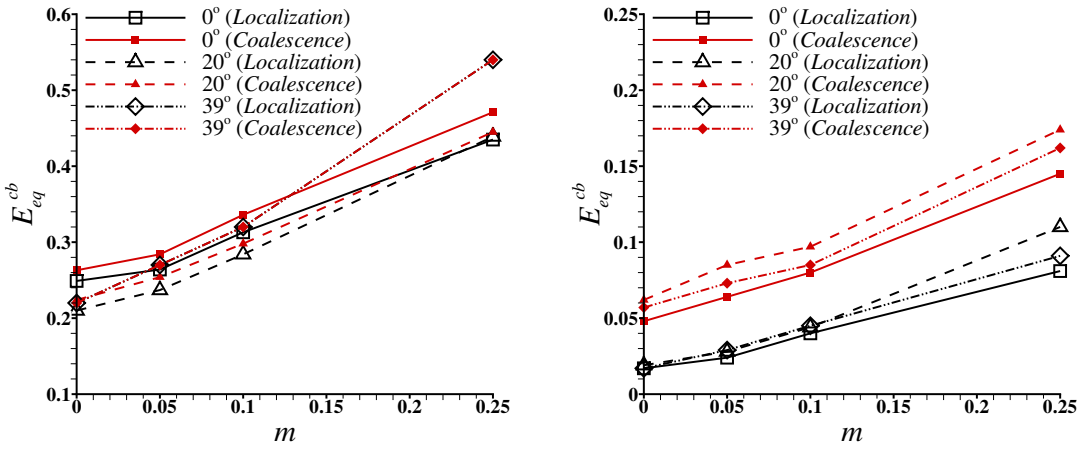

Figure 8: Variation of the critical equivalent strain, E_{eq}^{cb}, inside the band at the onset of localization/coalescence with material's strain rate sensitivity parameter, m, for (a) $T = 1.5$ and (b) $T = 2.75$.

Figs. 7 and 8, respectively, and the variation of E_{eq}^{cb} with imposed stress triaxiality, T, shown in Fig. 9.

As shown in Fig. 7, the value of E_{eq}^{c} increases with increasing value of strain rate sensitivity parameter, m, for all three initial orientation of the voided band, $\psi_u = 0°$, $20°$ and $39°$, and for both the imposed stress triaxiality values, $T = 1.5$ and 2.75. As also shown in the figure, for all three ψ_u values and for $T = 1.5$, the value of E_{eq}^{c} is same at the onset of localization and void coalescence. For $T = 2.75$, E_{eq}^{c} values at void coalescence are slightly greater than the values of E_{eq}^{c} at the onset of localization. This is consistent with the observation that at low imposed stress triaxiality values, the extent of void growth induced softening is not sufficient to trigger macroscopic localization, whereas at high imposed stress triaxiality values the void growth induced softening is sufficient to trigger macroscopic localization. As also shown in Fig. 7, the effect of initial band orientation on the value of E_{eq}^{c} depends on both, the values of T and m. For example, the minimum value of E_{eq}^{c} at the onset of localization corresponds to $\psi_u = 20°$ for $T = 1.5$ while it corresponds to $\psi_u = 39°$ for $T = 2.75$.

Similarly, the value of the critical equivalent strain in the band, E_{eq}^{cb}, at the onset of localization/coalescence increases with increasing value of m for all three ψ_u and for both T, Fig. 8. In addition, the variation of E_{eq}^{cb} with m for $T = 1.5$, Fig. 8(a), roughly follows the same trend as shown in Fig. 7(a) for E_{eq}^{c}. But for $T = 2.75$, the value of E_{eq}^{cb} at the onset of localization is less than the value of E_{eq}^{cb} at the onset of void coalescence for all the values of m and ψ_u, Fig. 8(b). For $T = 2.75$, the initial band orientation that gives lowest values of E_{eq}^{cb} is $\psi_u = 0°$, and the orientation that gives largest values of E_{eq}^{cb} is $\psi_u = 20°$. This is in contrast to the dependence of E_{eq}^{c} on ψ_u as shown in Fig. 7(b). This is because at high imposed stress triaxiality values, the onset of macroscopic localization occurs due to void growth induced softening that significantly affects the deformation in the band.

Figures 9(a) and (b) compare the variation of E_{eq}^{cb} at the onset of localization and coalescence, with imposed stress triaxiality values, T, for $m = 0.05$ and 0.25, respectively. As shown in

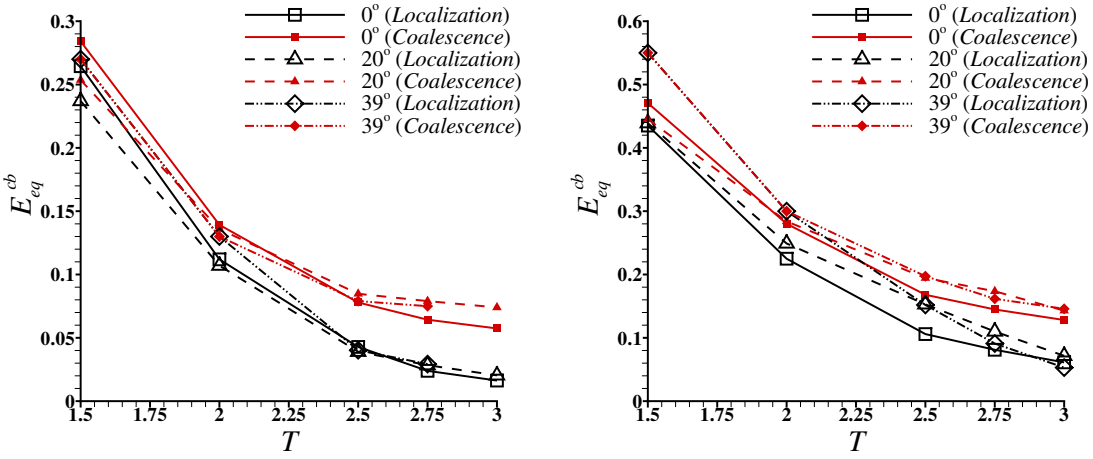

Figure 9: Variation of the critical equivalent strain, E_{eq}^{cb}, inside the band at the onset of localization/coalescence with imposed stress triaxiality, T, for (a) $m = 0.05$ and (b) $m = 0.25$.

the figure, for both the values of m, the value of E_{eq}^{cb} at localization/coalescence decreases with increasing value of the imposed T. But for sufficiently large values of T, with increasing T, the decrease in E_{eq}^{cb} at void coalescence is rather gradual as compared to the decrease in E_{eq}^{cb} at localization. This results in a clear separation between the values of E_{eq}^{cb} at localization and coalescence for $T \geq 2$, with the increasing difference between E_{eq}^{cb} at localization and coalescence with increasing value of T.

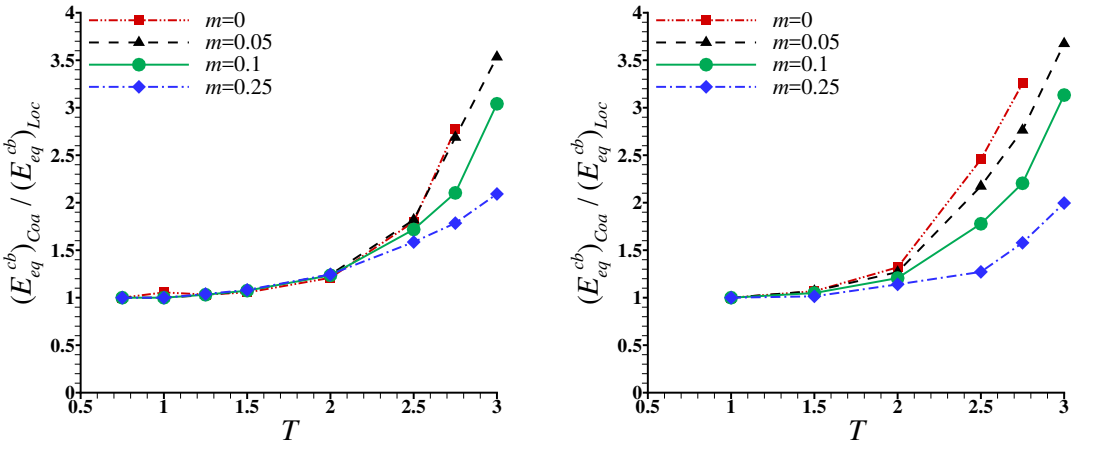

Figure 10: Variation in the ratio $(E_{eq}^{cb})_{coa}/(E_{eq}^{cb})_{Loc}$ with imposed stress triaxiality values, T, for initial orientation of the voided band, (a) $\psi_u = 0°$ and (b) $\psi_u = 20°$.

We now analyze the variation of the critical equivalent strain in the band at the onset of

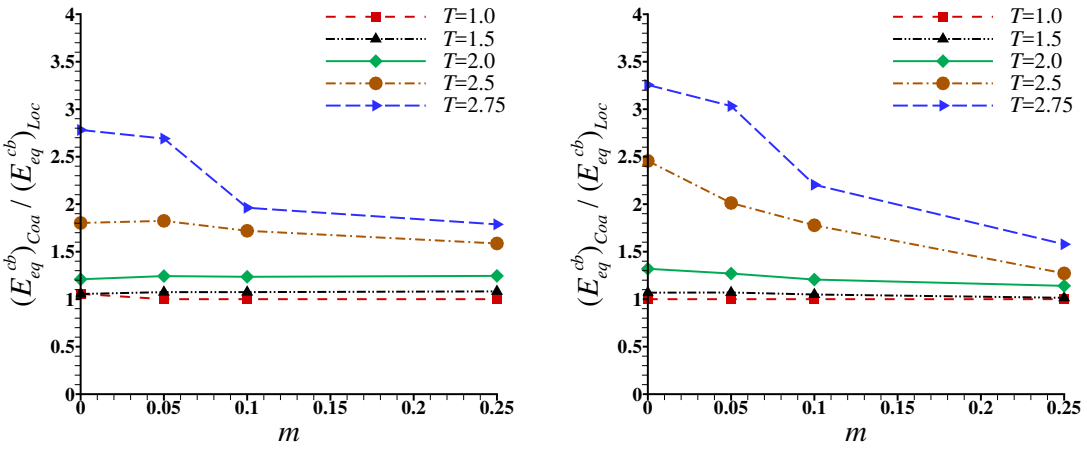

Figure 11: Variation in the ratio $(E_{eq}^{cb})_{coa}/(E_{eq}^{cb})_{Loc}$ with material's strain rate sensitivity parameter, m, for initial orientation of the voided band, (a) $\psi_u = 0°$ and (b) $\psi_u = 20°$.

coalescence normalized with the value of the critical equivalent strain in the band at the onset of localization, $(E_{eq}^{cb})_{Coa}/(E_{eq}^{cb})_{Loc}$, with T and m in Figs. 10 and 11, respectively, for two initial orientation of the voided band, ψ_u. As shown in Fig. 10, for all m and for both the values of ψ_u, the ratio $(E_{eq}^{cb})_{Coa}/(E_{eq}^{cb})_{Loc}$ is approximately one for $T < 2$ and for $T \geq 2$, the ratio $(E_{eq}^{cb})_{Coa}/(E_{eq}^{cb})_{Loc}$ increases with increasing value of T. This is because both $(E_{eq}^{cb})_{Coa}$ and $(E_{eq}^{cb})_{Loc}$ decrease with increasing T but for $T \geq 2$, $(E_{eq}^{cb})_{Loc}$ decreases more rapidly with increasing T than $(E_{eq}^{cb})_{Coa}$. Furthermore, as shown in Fig. 11, for $T > 2$, the value of $(E_{eq}^{cb})_{Coa}/(E_{eq}^{cb})_{Loc}$ decreases with increasing m for both the values of ψ_u. The decrease in the value of $(E_{eq}^{cb})_{Coa}/(E_{eq}^{cb})_{Loc}$ with increasing m becomes more pronounced with increasing value of the imposed T. Note, that both $(E_{eq}^{cb})_{Coa}$ and $(E_{eq}^{cb})_{Loc}$ increase with increasing m, thus a decrease in the value of $(E_{eq}^{cb})_{Coa}/(E_{eq}^{cb})_{Loc}$ suggests that $(E_{eq}^{cb})_{Loc}$ increases more rapidly with increasing m for higher stress triaxiality values. To summarize, the relative stabilizing effect induced by strain rate sensitivity of the material not only increases with the increasing value of the imposed stress triaxiality, but also the relative stabilizing effect of the strain rate sensitivity is greater at the onset of strain localization than at the onset of void coalescence.

3.4. Effect of Strain Hardening

In this work, we have focused on answering the question: How does the materials strain rate sensitivity affect the two mechanisms of macroscopic localization or ductile failure as a function of the imposed stress triaxiality? To answer this question, we have carried out a series of unit cell calculations, where the matrix material of the unit cell is considered to follow a strain rate dependent elastic perfectly plastic flow response. So the question arises as to what extent strain hardening in the material affects our results. A complete study of the combined effect of material's strain rate sensitivity, strain hardening and imposed stress triaxiality is beyond the scope of this work. However, our limited unit cell calculations presented in this section show that incorporating both material's strain rate sensitivity and strain hardening does not affect the qualitative effect

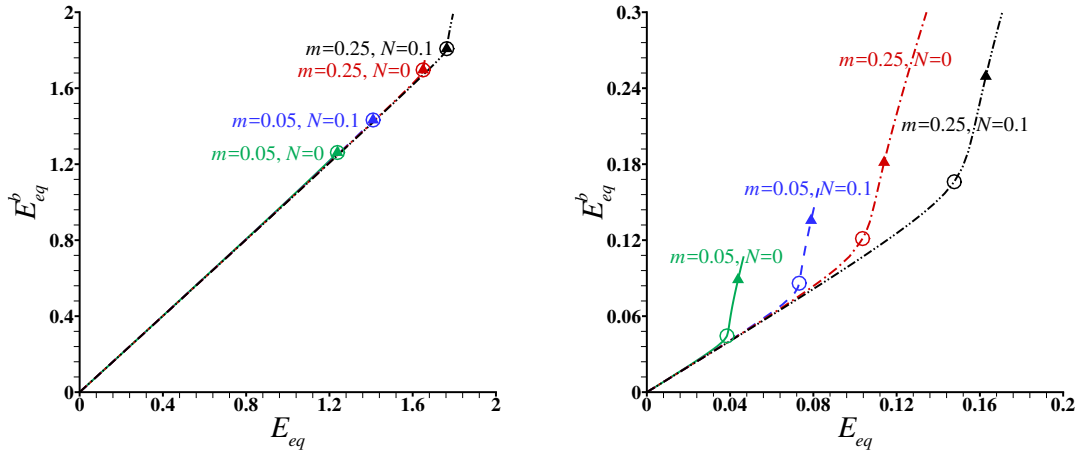

(a) (b)

Figure 12: A comparison of the evolution of equivalent strain in the band, E^b_{eq}, with macroscopic equivalent strain outside the band, E_{eq}, in strain hardening and non strain hardening materials for (a) imposed stress triaxiality, $T = 0.75$ and (b) $T = 2.5$. The initial orientation of the voided band is $\psi_u = 0^\circ$ for all the cases shown. In the figures the open circles mark the onset of localization while the closed triangles mark the onset of void coalescence.

of material's strain rate sensitivity and stress triaxiality reported in this work.

The results of our limited unit cell calculations to explore the combined effect of material's strain rate sensitivity, strain hardening and stress triaxiality on the two mechanisms of macroscopic localization is shown in Fig. 12. The combined effect of material's strain rate sensitivity and strain hardening is explored using the flow response given as,

$$\bar{\sigma} = \begin{cases} E\varepsilon & \varepsilon \leq \varepsilon_0 \\ \sigma_0 \cdot (\frac{\varepsilon^p}{\varepsilon_0})^N \cdot (1 + (\frac{\dot{\varepsilon}^p}{\dot{\varepsilon}_0})^m) & \varepsilon > \varepsilon_0 \end{cases} \tag{19}$$

instead of Eq. (17). For the calculations corresponding to results in Fig. 12, the values of $E = 167GPa$, $\sigma_0 = 418MPa$, $\varepsilon_0 = 0.0025$, $\dot{\varepsilon}_0 = 1\ s^{-1}$, $N = 0$ and 0.1, and $m = 0.05$ and 0.25 are used in Eq. (19). The results presented in Fig. 12 show that incorporating strain hardening in to the flow response of the material does not affect the qualitative effect of material's strain rate sensitivity and stress triaxiality on the onset of localization and void coalescence reported in this work. For example, irrespective of the value of the strain hardening exponent, N: (i) for low stress triaxiality value, $T = 0.75$, the value of E^b_{eq} at the onset of localization and void coalescence are the same, (ii) the value of E^b_{eq} at the onset of localization and void coalescence increases with the increasing value of strain rate sensitivity parameter, m, for both the values of T, (iii) for high stress triaxiality value, $T = 2.5$, the value of E^b_{eq} at the onset of localization is less than the value of E^b_{eq} at the onset of void coalescence, and (iv) the difference between the values of E^b_{eq} at the onset of localization and void coalescence decreases with increasing value of m.

4. Summary and Concluding Remarks

Strain localization and void coalescence (resulting in the formation of micro-cracks) in a porous ductile material mark the end of uniform deformation and limits the ductility of the material. In this work the focus is confined to analyzing the influence of material's strain rate sensitivity on the onset of strain localization and void coalescence as a function of the imposed stress triaxiality. To this end, three dimensional finite element calculations of unit cells have been carried out to model localization and coalescence in an infinite block containing a periodic distribution of initially spherical voids in a band. The unit cell modeled consists of a central block with a single void in its center within two semi-infinite void-free blocks. The matrix material of the unit cell is considered to follow a strain rate dependent elastic perfectly plastic flow response. Limited calculations have also been carried out to explore the combined effect of material's strain rate sensitivity and strain hardening. The unit cell calculations are carried out for one initial void volume fraction ($f_0 = 0.001$), a range of strain rate sensitivity parameter (varying in the range $0 \leq m \leq 0.25$), a range of imposed stress triaxiality (varying in the range $0.75 \leq T \leq 3$) with one Lode parameter ($L = -1$), and three initial orientations of the voided band ($\psi_u = 0°$, $20°$ and $39°$). In the calculations, onset of localization is defined as the point in the deformation history when the ratio of the rate of deformation in the band and outside the band reaches a critical level, while the onset of coalescence is defined when the ratio of the maximum to the minimum effective plastic strain rate at the surface of the void reaches a critical value following the work of Tekoğlu et al. (2015). Our results show that both the critical void volume fraction and strain, at the onset of localization and coalescence, are strongly influenced by the material's strain rate sensitivity and the imposed stress triaxiality.

The main conclusions of this work are as follows:

1. Influence of material's strain rate sensitivity, m, and imposed stress triaxiality, T, on the critical void volume fraction, f_c, at the onset of strain localization and void coalescence:
   (a) For low T values, f_c is roughly the same at the onset of localization and coalescence, whereas for greater values of T, f_c at the onset of coalescence is greater than f_c at the onset of localization.
   (b) For all values of T, the value of f_c at localization/coalescence increases with increasing m.
2. Influence of material's strain rate sensitivity, m, and imposed stress triaxiality, T, on the critical equivalent strain in the band, E_{eq}^{cb}, at the onset of strain localization and void coalescence:
   (a) For low T values, $T < 2$, E_{eq}^{cb} is same at the onset of localization and coalescence, whereas for $T \geq 2$, E_{eq}^{cb} at the onset of coalescence is greater than E_{eq}^{cb} at the onset of localization.
   (b) For all values of m, the value of E_{eq}^{cb} at the onset of localization/coalescence decreases with increasing T. But for $T \geq 2$, the value of E_{eq}^{cb} at localization decreases more rapidly with increasing T compared to the value of E_{eq}^{cb} at coalescence.
   (c) For all values of T, the value of E_{eq}^{cb} at the onset of localization/coalescence increases with increasing value of m. But for $T \geq 2$, the value of E_{eq}^{cb} at localization increases more with increasing value of m compared to the value of E_{eq}^{cb} at coalescence.

(d) The concluding points, 2(b) and (c), clearly show that the relative stabilizing effect of m increases with the increasing value of T, and the relative stabilizing effect of m is greater at the onset of localization than at the onset of coalescence.

Our limited results aimed at exploring the combined effect of material's strain rate sensitivity, strain hardening and imposed stress triaxiality on the onset of localization and void coalescence show that incorporating strain hardening into the flow response of the material does not affect the aforementioned qualitative effect of material's strain rate sensitivity and stress triaxiality on the onset of localization and void coalescence. In this work, we have focused on one Lode parameter value, $L = -1$. The value of the Lode parameter may also affect the onset of localization and void coalescence especially at low values of stress triaxiality. The numerical method presented in this work can be used for future research to explore the combined effect of material's strain rate sensitivity and strain hardening, and imposed stress triaxiality and Lode parameter on the onset of localization and void coalescence. Furthermore, our results motivate the need to incorporate the effect of material's strain rate sensitivity in the porosity and stress triaxiality dependent flow potential (or constitutive response) of the material.

Acknowledgements

The financial support provided by the European Union's Horizon2020 Programme (Excellent Science, Marie-Sklodowska - Curie Actions, H2020 - MSCA - RISE - 2017) under REA grant agreement 777896 (Project QUANTIFY) are gratefully acknowledged. Shmuel Osovski would also like to acknowledge the financial support of the Pazy foundation (Young researchers award grant no. 1176). We are thankful to Dr. J.A. Rodríguez-Martínez of University Carlos III of Madrid for numerous fruitful discussions. The authors also acknowledge to Katarzyna Kowalczyk-Gajewska from Institute of Fundamental Technological Research, Polish Academy of Sciences, for helpful discussions.

Appendix A. Procedure for the Multipoint constraint

The procedure to prescribe proportional loading i.e. fixed ratio of principal stresses, $R = \Sigma_2/\Sigma_1$ and $Q = \Sigma_3/\Sigma_1$ to maintain constant macroscopic stress triaxiality, T, and Lode parameter, L, throughout the deformation history, follows the work of Vadillo et al. (2016).

Since the macroscopic true stresses (Σ_1, Σ_2, Σ_3) and the macroscopic strain rates ($\dot{E}_1$, $\dot{E}_2$, $\dot{E}_3$) are equal to the volume average values in a cell (Hill, 1967), the total rate of deformation work in the whole cell $\dot{W}$ considering jointly upper, lower and central voided block, can be written as:

$$\dot{W} = V\Sigma_1\dot{E}_1 + V\Sigma_2\dot{E}_2 + V\Sigma_3\dot{E}_3 \tag{A.1}$$

where V is the total volume of the RVE.

Defining $P_1 = V\Sigma_1$, $P_2 = V\Sigma_2$ and $P_3 = V\Sigma_3$ as generalized forces and work rate conjugate quantities to $\dot{E}_1$, $\dot{E}_2$ and $\dot{E}_3$, respectively, the expression of $\dot{W}$ becomes:

$$\dot{W} = P_1\dot{E}_1 + P_2\dot{E}_2 + P_3\dot{E}_3 \tag{A.2}$$

in which P_1, P_2 and P_3 must satisfy:

$$\frac{P_2}{P_1} = R; \qquad \frac{P_3}{P_1} = Q \tag{A.3}$$

The ratios R and Q can be written in terms of the imposed stress triaxiality, T, and Lode parameter, L:

$$Q = \frac{3T\sqrt{L^2+3} - 3 - L}{3T\sqrt{L^2+3} + 3 - L}; \qquad R = \frac{3T\sqrt{L^2+3} + 2L}{3T\sqrt{L^2+3} + 3 - L} \tag{A.4}$$

Next, with the transformation:

$$\begin{pmatrix} \dot{E}_{(I)} \\ \dot{E}_{(II)} \\ \dot{E}_{(III)} \end{pmatrix} = \mathbf{N} \begin{pmatrix} \dot{E}_1 \\ \dot{E}_2 \\ \dot{E}_3 \end{pmatrix}; \qquad \begin{pmatrix} P_{(I)} \\ P_{(II)} \\ P_{(III)} \end{pmatrix} = \mathbf{N} \begin{pmatrix} P_1 \\ P_2 \\ P_3 \end{pmatrix} \tag{A.5}$$

where $\mathbf{N}$ is an orthonormal $\left(\mathbf{N}^{-1} = \mathbf{N}^T\right)$ unsymmetric matrix:

$$\mathbf{N} = \begin{pmatrix} A_{11} & A_{12} & A_{13} \\ A_{21} & A_{22} & A_{23} \\ A_{31} & A_{32} & A_{33} \end{pmatrix};$$

with the elements:

$$\begin{aligned}
A_{11} &= \frac{1}{\sqrt{1+R^2+Q^2}}; \quad A_{12} = \frac{R}{\sqrt{1+R^2+Q^2}}; \quad A_{13} = \frac{Q}{\sqrt{1+R^2+Q^2}} \\
A_{21} &= -\frac{R}{\sqrt{1+R^2}}; \qquad A_{22} = \frac{1}{\sqrt{1+R^2}}; \qquad A_{23} = 0. \\
A_{31} &= \frac{Q}{\sqrt{(1+R^2)\,(1+R^2+Q^2)}}; \quad A_{32} = \frac{RQ}{\sqrt{(1+R^2)\,(1+R^2+Q^2)}} \\
A_{33} &= -\frac{(1+R^2)}{\sqrt{(1+R^2)\,(1+R^2+Q^2)}}
\end{aligned} \tag{A.6}$$

Now, $\dot{W}$ can be expressed in terms of the transformed rates of deformation and forces, as:

$$\dot{W} = P_{(I)}\dot{E}_{(I)} + P_{(II)}\dot{E}_{(II)} + P_{(III)}\dot{E}_{(III)} \tag{A.7}$$

If in the transformed coordinate system, the imposed incremental boundary conditions are prescribed as stress uniaxial:

$$P_{(II)} = 0; \quad P_{(III)} = 0; \quad \dot{E}_{(I)} = \dot{E}_I \tag{A.8}$$

the total rate of deformation work has the form $\dot{W} = P_{(I)}\dot{E}_I$, that follows, in the initial system and considering the relations given in Eq. (A.5), the three relations:

$$\begin{aligned} &(1) \quad P_{(II)} = 0 \rightarrow \quad A_{21}P_1 + A_{22}P_2 + A_{23}P_3 = 0 \\ &(2) \quad P_{(III)} = 0 \rightarrow \quad A_{31}P_1 + A_{32}P_2 + A_{33}P_3 = 0 \\ &(3) \quad \dot{E}_{(I)} = \dot{E}_I \rightarrow \; A_{11}\dot{E}_1 + A_{12}\dot{E}_2 + A_{13}\dot{E}_3 = \dot{E}_I \end{aligned} \tag{A.9}$$

or in a similar manner, if values of R, Q and $\dot{E}_I$ are prescribed on the unit cell, this leads to:

$$\begin{aligned} &(1) \quad (\Sigma_2/\Sigma_1) = R \\ &(2) \quad (\Sigma_3/\Sigma_1) = Q \\ &(3) \quad \left(\dot{E}_1 + R\dot{E}_2 + Q\dot{E}_3\right) = \dot{E}_I\sqrt{1 + R^2 + Q^2} \end{aligned} \tag{A.10}$$

This procedure was implemented into ABAQUS/Standard (2017) as MPC user subroutine.

References

ABAQUS/Standard, 2017. Simulia, User's Manual, version 6.17 Edition. Dassault Systémes, Providence, USA.

Agoras, M., Ponte Castañeda, P., 2014. Anisotropic finite-strain models for porous viscoplastic materials with microstructure evolution. International Journal of Solids and Structures 51, 981–1002.

Aretz, H., 2007. Numerical analysis of diffuse and localized necking in orthotropic sheet metals. International Journal of Plasticity 23, 798–840.

Barsoum, I., Faleskog, J., 2011. Micromechanical analysis on the influence of the lode parameter on void growth and coalescence. International Journal of Solids and Structures 48 (6), 925–938.

Besson, J., Steglich, D., Brocks, W., 2003. Modeling of plane strain ductile rupture. International Journal of Plasticity 19 (10), 1517–1541.

Brünig, M., Gerke, S., Hagenbrock, V., 2013. Micro-mechanical studies on the effect of the stress triaxiality and the lode parameter on ductile damage. International Journal of Plasticity 50, 49–65.

Budiansky, B., Hutchinson, J., Slutsky, S., 1982. Void growth and collapse in viscous solids. in: H.G. Hopkins and M.J. Sewell, eds., Mechanics of Solids, Pergamon Press, Oxford, 13–45.

Cheng, F., Kim, S.-M., Reddy, J., Al-Rub, R. K. A., 2014. Modeling of elastoplastic behavior of stainless-steel/bronze interpenetrating phase composites with damage evolution. International Journal of Plasticity 61, 94–111.

Cocks, A., Ashby, M., 1982a. Creep fracture by coupled power-law creep and diffusion under multiaxial stress. Metal Science 16, 465–474.

Cocks, A., Ashby, M., 1982b. On creep fracture by void growth. Progress in Material Science 27, 189–244.

Czarnota, C., Mercier, S., Molinari, A., 2006. Modelling of nucleation and void growth in dynamic pressure loading, application to spall test on tantalum. International Journal of Fracture 141, 177–194.

Dunand, M., Mohr, D., 2014. Effect of lode parameter on plastic flow localization after proportional loading at low stress triaxialities. Journal of the Mechanics and Physics of Solids 66, 133–153.

Duva, J., 1986. A constitutive description of nonlinear materials containing voids. Mechanics of Materials 5, 317–329.

Fressengeas, C., Molinari, A., 1985. Inertia and thermal effects on the localization of plastic flow. Acta Metallurgica 33, 387–396.

Fritzen, F., Forest, S., Böhlke, T., Kondo, D., Kanit, T., 2012. Computational homogenization of elasto-plastic porous metals. International Journal of Plasticity 29, 102–119.

Ghosh, A., 1977. Tensile instability and necking in materials with strain hardening and strain-rate hardening. Acta Metallurgica 25, 1413–1424.

Guo, T., Wong, W., 2018. Void-sheet analysis on macroscopic strain localization and void coalescence. Journal of the Mechanics and Physics of Solids 118, 172–203.

Hill, R., 1967. The essential structure of constitutive laws for metal composites and polycrystals. Journal of the Mechanics and Physics of Solids 15, 79–95.

Hutchinson, J., Neale, K., 1977. Influence of strain-rate sensitivity on necking under uniaxial tension. Acta Metall 25, 839–846.

Hutchinson, J., Neale, K., Needleman, A., 1978. Sheet necking-I. validity of plane stress assumptions of the long wavelength approximation. In: Koistinen, D.P., Wang, N.W. (Eds.), Mechanics of Sheet Metal Forming, New York: Plenum Publishing Corp, 111–126.

Koplik, J., Needleman, A., 1988. Void growth and coalescence in porous plastic solids. International Journal of Solids and Structures 24 (8), 835–853.

Liu, Z., Wong, W., Guo, T., 2016. Void behaviors from low to high triaxialities: Transition from void collapse to void coalescence. International Journal of Plasticity 56, 183–202.

Luo, T., Gao, X., 2018. On the prediction of ductile fracture by void coalescence and strain localization. Journal of the Mechanics and Physics of Solidss 113, 82–104.

Marciniak, Z., Kuczyński, K., 1967. Limit strains in the processes of stretch-forming sheet metal. International Journal of Mechanical Sciences 9, 609–620.

Marciniak, Z., Kuczyński, K., Pokora, T., 1973. Influence of the plastic properties of a material on the forming limit diagram for sheet metal in tension. International Journal of Mechanical Sciences 15, 789–800.

Mear, M., Hutchinson, J., 1985. Influence of yield surface curvature on flow localization in dilatant plasticity. Mechanics of Materials 4, 395–407.

Mercier, S., Molinari, A., 2003. Predictions of bifurcations and instabilities during dynamic extensions. International Journal of Solids and Structures 40, 1995–2016.

Nahshon, K., Hutchinson, J., 2008. Modification of the gurson model for shear failure. European Journal of Mechanics A-Solid 27, 1–17.

Needleman, A., Rice, J., 1978. Limits to ductility set by plastic flow localization. in: D.P. Koistinen et al., eds., Mechanics of Sheet Metal Forming, Plenum Publishing, New York, 237–367.

Nemat-Nasser, S., lwakuma, T., Accorsi, M., 1986. Cavity growth and grain boundary sliding in polycrystalline solids. Mechanics of Materials 5, 137–144.

Ortiz, M., Molinari, A., 1992. Effect of strain hardening and rate sensitivity on the dynamic growth of a void in a plastic material. Journal of Applied Mechanics 114, 48–53.

Osovski, S., Srivastava, A., Ponson, L., Bouchaud, E., Tvergaard, V., Ravi-Chandar, K., Needleman, A., 2015. The effect of loading rate on ductile fracture toughness and fracture surface roughness. Journal of the Mechanics and Physics of Solids 76, 20–46.

Pan, J., 1983a. Perturbation analysis of shear strain localization in rate sensitive materials. International Journal of Solids and Structures 19, 153–164.

Pan, J., Saje, M., Needleman, A., 1983. Localization of deformation in rate-sensitive porous plastic solids. International Journal of Fracture 21, 261–278.

Pan, J.and Rice, J., 1983b. Rate sensitivity of plastic flow and implications for yield surface vertices. International Journal of Solids and Structures 19, 973–987.

Pardoen, T., Hutchinson, J., 2000. An extended model for void growth and coalescence. Journal of the Mechanics and Physics of Solids 48, 2467–2512.

Pineau, A., Benzerga, A., Pardoen, T., 2016. Failure of metals i: Brittle and ductile fracture. Acta Materialia 107, 424–483.

Rice, J., 1977. The localization of plastic deformation. In: Koiter, W.T., (Ed.), Theoretical and Applied Mechanics, North-Holland, 207–220.

Rudnicki, J., Rice, J., 1975. Conditions for the localization of deformation in pressuresensitive dilatant materials. Journal of the Mechanics and Physics of Solids 23, 371–394.

Saje, M., Pan, J., Needleman, A., 1982. Void nucleation effects on shear localization in porous plastic solids. International Journal of Fracture 19, 163–182.

Scheyvaerts, F., Onck, P., Tekoğlu, C., Pardoen, T., 2011. The growth and coalescence of ellipsoidal voids in plane strain under combined shear and tension. Journal of the Mechanics and Physics of Solids 59, 373–397.

Srivastava, A., Needleman, A., 2013. Void growth versus void collapse in a creeping single crystal. Journal of the Mechanics and Physics of Solids 61 (5), 1169–1184.

Srivastava, A., Ponson, L., Osovski, S., Bouchaud, E., Tvergaard, V., Needleman, A., 2014. Effect of inclusion density on ductile fracture toughness and roughness. Journal of the Mechanics and Physics of Solids 63, 62–79.

Taya, M., Seidel, E., 1981. Void growth in a viscous metal. International Journal of Engineering Science 19, 1083–1094.

Tekoğlu, C., Hutchinson, J., Pardoen, T., 2015. On localization and void coalescence as a precursor to ductile fracture. Phil. Trans. R. Soc. A 373 (2038), 20140121.

Torki, M., Tekoğlu, C., Leblond, J., Benzerga, A., 2017. Theoretical and numerical analysis of void coalescence in porous ductile solids under arbitrary loadings. International Journal of Plasticity 91, 160–181.

Tvergaard, V., 1981. Influence of voids on shear band instabilities under plane strain conditions. International Journal of Fracture 17, 389–407.

Tvergaard, V., 1982. On localization in ductile materials containing spherical voids. International Journal of fracture 18 (4), 237–252.

Tvergaard, V., 1989. Numerical study of localization in a void-sheet. International journal of solids and structures 25 (10), 1143–1156.

Vadillo, G., Reboul, J., Fernández-Sáez, J., 2016. A modified gurson model to account for the influence of the lode parameter at high triaxialities. European Journal of Mechanics A/Solids 56, 31–44.

Vadillo, G., Rodríguez-Martínez, J., Fernández-Sáez, J., 2012. On the interplay between strain rate and strain rate sensitivity on flow localization in the dynamic expansion of ductile rings. International Journal of Solids and Structures 49, 481–491.

Wang, H., Wu, P., Kurukuri, S., Worswick, M. J., Peng, Y., Tang, D., Li, D., 2018. Strain rate sensitivities of deformation mechanisms in magnesium alloys. International Journal of Plasticity 107, 207–222.

Yamamoto, H., 1978. Conditions for shear localization in the ductile fracture of void-containing materials. International Journal of Fracture 14, 347–365.

Yoon, H., Taya, M., 1984. Prediction of the void growth at its early stage in a viscous two-phase material. International Journal of Engineering Science 22, 1035–1040.